

Improving the description of interlayer bonding in TiS_2 by Density Functional Theory

Matteo Ricci, Alberto Ambrosetti, and Pier Luigi Silvestrelli*

*Dipartimento di Fisica e Astronomia "G. Galilei", Università di Padova, via Marzolo 8,
I-35131, Padova, Italy.*

E-mail: psil@pd.infn.it

Abstract

We investigate energetic and electronic properties of TiS_2 , an archetypal van der Waals (vdW) material, from first principles, in the framework of the Density Functional Theory (DFT). In this system a recent experimental study showed a puzzling discrepancy between the distribution of the electron density in the interlayer region obtained by X-ray diffraction data and that computed by DFT, even adopting DFT functionals that should properly include vdW effects. Such a discrepancy could indicate a partial failure of state-of-the-art DFT approaches in describing the weak interlayer interactions of TiS_2 and, possibly, of similar systems too. In order to shed light on this issue, we have carried out simulations based on different DFT functionals, basically confirming the mentioned discrepancy with the experimental findings. Subsequently, we have tried to reproduce the experimental interlayer electronic density deformation both by changing the parameters characterizing the rVV10 DFT functional (in such a way to artificially modify the strength of the vdW interactions at short or long range), and also by adopting a modified pseudopotential for Sulfur atoms, involving d orbitals. The latter approach turns out to be particularly promising. In fact, using this novel, more flexible pseudopotential, we obtain not only an electronic density deformation closer to the experimental profile, but also a better estimate of the interlayer binding energy. Interestingly, this improvement in the theoretical DFT description is not limited to TiS_2 but also applies to other similar layered systems involving S atoms, such as TaS_2 , HfS_2 , and MoS_2 .

1 Introduction

First identified in 1873,¹ the van der Waals (vdW) interactions are forces that today attract more interest than ever. They are present everywhere, but their manifestations still pose challenging questions which are relevant for such varied systems as soft matter, surfaces, and DNA, and in phenomena as different as supramolecular binding, surface reactions, and the dynamic properties of water. vdW interactions play a central role even in the characterization of layered materials, such as transition metal dichalcogenides (TMDs). These represent a large class of materials with mild stiffness, which are not as soft as tissues and not as strong as metals.² They are two-dimensional systems which have unique properties and are central to current research in solid-state science. In TMDs, a transition metal atom (M) layer is sandwiched between two chalcogen atom (X) layers and it is commonly assumed that the MX_2 slabs are stacked by vdW interactions, whereas the intralayer M-X interactions are instead covalent. The weak, interlayer vdW interactions play a key role in the formation, intercalation, exfoliation and layer-by-layer building of TMD materials, as well as being decisive for their characteristic properties.

Like all non-relativistic electronic effects, the vdW interactions are present in the (unknown) exact Density Functional Theory (DFT) exchange-correlation (XC) functional, but they are not properly described by standard approximate DFT schemes, such as local density approximation (LDA)³ or semilocal generalized gradient approximation (GGA).⁴ Hence the need to introduce truly non local XC functionals, able to accurately account for vdW corrections, arises. Despite a considerable amount of work focused on the development of accurate vdW-corrected DFT methods, a precise characterization of the layer-layer distance and of the interlayer binding energy of vdW layered materials, still represents a challenging issue.⁵⁻⁹ This is due to the nonlocal and long-range nature of the vdW interaction, as well as to the coexistence of the weak vdW bonding and much stronger intralayer chemical bonding. Fully accounting for the vdW interaction is achievable by high-level methods such as quantum Monte Carlo (QMC),¹⁰ coupled-cluster singles and doubles with perturbative

triples (CCSD(T)),¹¹ and exploiting the adiabatic-connection fluctuation-dissipation theorem within the random-phase approximation (RPA),¹² which are, however, only feasible for limited-size systems because of their high computational cost.

The physical quantity lying at the DFT core, is the electron density (ED), which fully determines the total energy of any many-electron system in its ground state. The ED distribution probably represents the most information-rich observable available since it has become possible to determine EDs from analysis of structure factors obtained from accurate X-ray diffraction data. During the past decade, the accuracy of experimental X-ray diffraction data has increased dramatically owing to the use of high-energy synchrotron sources, which significantly limit systematic errors in the data and, thanks to these modern techniques, nowadays it is possible to evaluate both structural and electronic properties of a wide class of layered materials in an extremely accurately way. In this respect, Medvedev *et al.*¹³ have pointed out that modern DFT functionals are constructed on the basis of empirical fitting on energetic and geometrical benchmarks, neglecting the ED as a parameterization parameter. If, from one side, this leads to improved predictions of energetic and structural features, from the other, the exact reproduction of the ED has worsened. In a recent study, Kasai *et al.*¹⁴ studied the archetypal vdW material, TiS₂, to compare the ED distribution derived from X-ray diffraction data with the theoretical one obtained by several DFT functionals. They obtained a good agreement between theory and experiment for the description of the intralayer, covalent Ti-S interaction, but, at the same time, significant discrepancies were found for the interlayer vdW interactions, particularly considering the ED distribution in the region between S atoms belonging to adjacent layers. In fact, while the properties at the bond critical point (BCP) were quite similar, noticeable differences were instead observed away from the BCP: considering the theoretical DFT density, the S atoms behave as if they are practically not interacting with the neighboring layer, showing charge concentration and accumulation in the region expected for a lone pair in an *sp*³-hybridized S atom with three

bonds to nearby Ti atoms and no other bonds; in the experiment, however, an appreciable charge accumulation and concentration was observed in the interlayer region, which was interpreted as a sign of a stronger and more directional interaction between S atoms. Thus, this study suggested the inability of current DFT functionals to accurately describe the interlayer ED for vdW layered materials, thus supporting the conclusions of Medvedev *et al.* In order to shed light on this issue, in the first part of this study, we apply the LDA, the semilocal PBE⁴ and the vdW-corrected rVV10¹⁵ DFT functionals, with standard Projector-Augmented Wave (PAW) pseudopotentials,¹⁶ to explore the behavior of the interlayer ED in different regimes, obtained by also modifying the parameters of the rVV10 functional, so that to artificially tuning the intensity of the vdW interactions. The basic result is that, in order to produce an ED distribution appreciably closer to the experimental profile, we have to select the rVV10 parameters in such a way to unphysically increase the strength of the vdW interactions, thus leading to an exaggeratedly high interlayer binding energy. In the second part a standard rVV10 approach is used, but a novel pseudopotential is adopted, which explicitly accounts for the $3d$ orbitals of the S atom. While these orbitals are empty in the isolated, neutral S atom, they can play a role¹⁷ in molecules and condensed-matter systems where S atoms interact with other atoms and form bonds. Interestingly, using this novel, more flexible S pseudopotential, we obtain not only an ED distribution closer to the experimental profile, but also a better estimate of the interlayer binding energy. We finally show that this improvement in the theoretical DFT description is not limited to TiS₂ but also applies to other, similar layered systems involving S atoms, such as TaS₂, HfS₂, and MoS₂.

2 Theoretical background and Computational details

In DFT the properties of a many-electron system can be determined by introducing suitable functionals of the electron density $n(\mathbf{r})$; the most interesting many-body physical effects are

described by the so-called exchange-correlation (XC) functional, related to the XC potential: $V_{xc}[n(\mathbf{r})] = V_x[n(\mathbf{r})] + V_c[n(\mathbf{r})]$. In principle V_{xc} describes all the many-body effects, including the vdW interactions, however, in practice, a number of approximation must be introduced, since, unfortunately, the exact form of the XC functional is not known. Nowadays several kinds of approaches to approximately include vdW interaction in DFT calculations are available. Some of these are based on semiempirical, atom-based pair potentials, able to give approximate vdW corrections;¹⁸⁻²⁰ instead others are built introducing a suitable non-local XC density functional, such as the vdW-DF family by Dion *et al.*²¹ and the scheme proposed by Vydrov and Van Voorhis,²² with the revised, more efficient version rVV10.¹⁵ rVV10 certainly represents one of the best vdW-corrected functionals nowadays available; it takes into account the entire range of vdW interactions at a reasonable computational cost using only the ED $n(\mathbf{r})$ as input. In particular, the rVV10 non-local correlation energy has the following expression:

$$E_c^{NL} = \int \int n(\mathbf{r})\Phi(\mathbf{r}, \mathbf{r}')n(\mathbf{r}') \quad (1)$$

where Φ is the non-local correlation kernel, which is:

$$\Phi = -\frac{3e^4}{2m^2} \frac{1}{(q(\mathbf{r})R^2 + 1)(q(\mathbf{r}')R^2 + 1)[(q(\mathbf{r}) + q(\mathbf{r}'))R^2 + 2]} \quad (2)$$

In the above expression $R = |\mathbf{r} - \mathbf{r}'|$ and $q(\mathbf{r})$ is a function of the ED and its gradient:

$$q(\mathbf{r}) = \frac{\omega_0(n(\mathbf{r}), \nabla n(\mathbf{r}))}{k(n(\mathbf{r}))} \quad (3)$$

where

$$\omega_0 = \sqrt{C \frac{\hbar^2}{m^2} \left| \frac{\nabla n(\mathbf{r})}{n(\mathbf{r})} \right|^4 + \frac{1}{3} \frac{4\pi n(\mathbf{r})e^2}{m}} \quad (4)$$

and

$$k(n(\mathbf{r})) = 3\pi b \left(\frac{n(\mathbf{r})}{9\pi} \right)^{1/6}. \quad (5)$$

The total XC functional is then obtained by adding the non-local correlation energy to the refitted Perdew-Wang exchange functional²³ and the Perdew-Wang LDA correlation²⁴ functional, as proposed in the seminal work by Vydrov and Van Voorhis:²²

$$E_{xc}^{NL} = E_x^{rPW86} + E_c^{LDA} + E_c^{NL} . \quad (6)$$

The rPW86 exchange functional was chosen mainly because it is nearly vdW-free,²³ in such a way to avoid double-counting effects. In eq. (4) the C parameter represents the so-called local band gap and is tuned to give accurate asymptotic vdW C_6 coefficients, thus regulating the behavior of the long-range component of vdW interactions. The fitting procedure, aimed to minimize the average error for a benchmark set of 54 C_6 coefficients, was originally carried out by Vydrov and Van Voorhis,²² leading to an optimal value of $C = 0.0093$. Another essential aspect of the VV10 (and its successor rVV10) formalism is the presence of a second adjustable parameter, b (see eq. (5)), which controls the short range behavior of the non-local correlation energy. This means that when E_c^{NL} is added to the other energetic terms, the b parameter is adjusted to merge the interaction energy contributions at short and intermediate ranges. With an empirical fitting procedure on the S22 binding-energy data set,²⁵ Vydrov and Van Voorhis proposed a value of $b = 5.9$.²² After the implementation of the efficient Roman-Perez, Soler²⁶ interpolation scheme in the reciprocal space, this value was revised by Sabatini and coworkers to $b = 6.3$.¹⁵

We have chosen rVV10 as the basic DFT functional to investigate the effect of vdW interactions in the ED distribution of TiS_2 (although extensive tests were also performed using other vdW-corrected functionals), also because of the possibility to separately modify the intensity of both short- and long-range vdW interactions in a transparent way by simply tuning the two adjustable parameters b and C mentioned above. First the short-range component is analyzed. This is done by considering two different regimes: the former in which the value of the b parameter is increased to $b=10.0$, thus damping the intensity of short

range vdW interactions, and the latter in which b is reduced to $b=1.0$, that instead results in a substantial increase of the intensity of the short-range vdW interaction. While tuning the parameters of the rVV10 functional can improve the description of some properties of the TiS₂ system, clearly this could lead to a reduction of the transferability of the modified functional to other systems.

Our ab-initio calculations have been performed using the version 6.5 of the Quantum ESPRESSO (QE) DFT package.^{27,28} We first used for Ti and S atoms standard PAW¹⁶ pseudopotentials taken from the QE database.²⁹ Subsequently, for further testing, we have generated, for the S atom, a novel pseudopotential, using the *atomic* QE program. We report DFT results obtained using the LDA, the semilocal GGA PBE functional, and the vdW-corrected functional rVV10, both in its standard form and considering the variants (parameter changes and combination with a novel S pseudopotential) described above. Self-consistent calculations and relaxation processes, leading to the ground-state equilibrium geometry of bulk TiS₂, were carried out within the *PWscf* QE program. The calculations adopted plane-wave and density cutoffs of 100 and 1000 Ry, respectively, to get highly-converged results, a cold-smearing parameter of 0.01 Ry, and a $12 \times 12 \times 4$ k-point mesh for the sampling of the Brillouin Zone (BZ). The ED analysis is carried out using the *PostProc* QE program, employing the B-Spline method³⁰ for the $n(x, y, z)$ interpolation; in particular, for the ED profile computed along the S-S, S-center, and Ti-S lines, a real-space grid of $600 \times 600 \times 800$ (x, y, z) points, generated inside a parallelepiped containing the axis of interest, is used. To get a reliable estimate of the $\nabla^2 n(\mathbf{r})$ function, in the case of the S-S line, the distance between the parallelepiped axis and the edges of its sides is 0.5 Å, for the S-center case 0.25 Å, and finally 0.35 Å for the Ti-S line. The ED is then processed by using the *Critic2* program.^{31,32} More specifically, we compute the ED charge deformation, $\Delta n(\mathbf{r})$, by considering a spatial mesh of $72 \times 72 \times 108$ points inside the unit cell (containing one Ti atom and two S atoms) and taking the difference between the ED $n(\mathbf{r})$ and the sum of the EDs of the isolated Ti and S atoms. $\Delta n(\mathbf{r})$ profiles and Laplacian $\nabla^2 n(\mathbf{r})$ maps, in

the interlayer and intralayer areas, are then evaluated on the plane of interest using *Critic2*. The calculation of the atomic properties of a given S atom is carried out by making an integration of the so-called "atomic basin" of the S atom, represented by the space region whose surface has zero-density gradient flux. This is done again with the *Critic2* program, that allows to compute spherical multipolar moments defined as

$$Q_{lm} = \int_A n(\mathbf{r}) r^l Y_{lm} \quad (7)$$

where the integration domain A is the atomic basin volume. In the above equation, $n(\mathbf{r})$ is the charge ED and Y_{lm} are the spherical harmonics, in which the m index runs over the interval $[-l; l]$. With this definition, the magnitude of the dipole moment attributed to the S atom is obtained as the square root of the sum of the squared $l=1$ terms:

$$d(q_A) = \sqrt{\sum_{m=-1,0,1} Q_{1m}^2} . \quad (8)$$

3 Results and discussions

Starting from the experimental lattice parameters, $a = 3.398 \text{ \AA}$ and $c = 5.665 \text{ \AA}$, as reported by Kasai *et al.*,¹⁴ we relax the crystal structure in the intralayer atomic plane until the force acting on the system is smaller than 10^{-5} Ry/a.u. This relaxation process, carried out with both PBE and rVV10 functionals, leads to very similar results, as expected,¹⁴ since vdW interactions do not substantially influence the geometry of the intralayer plane. By further optimizing the interlayer geometry, the standard rVV10 functional predicts that the distance between two S atoms belonging to adjacent layers is 3.443 \AA while the intralayer S-Ti distance is 2.421 \AA , in excellent agreement with the reference DFT values (at the SCAN+rVV10 level³³) of 3.446 \AA and 2.420 \AA , respectively, reported in ref. 14. As already mentioned, Kasai *et al.*¹⁴ pointed out that DFT simulations are characterized by a an interlayer S-S ED deformation significantly lower than the experimental one, implying that the X-ray diffrac-

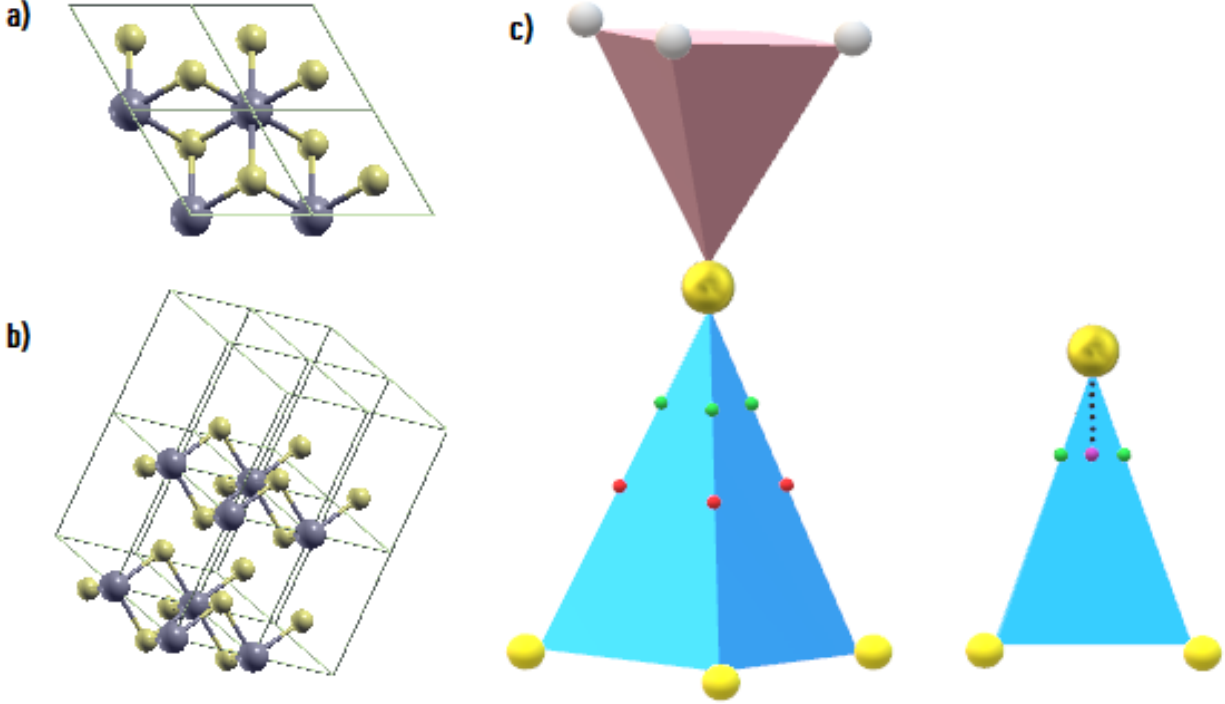


Figure 1: a) & b): bulk structure of TiS_2 . The unit cell is repeated twice along the x , y , and z directions. c) On the left hand side the TiS_2 octahedron is represented: the bigger S atom in the middle is the reference S atom, while the grey balls denote Ti atoms. The lower tetrahedron sides indicate the S-S lines, connecting the reference atom to the S atoms belonging to the adjacent layer. On the right hand side, the S-center line (connecting the reference S atom to the center of the lower tetrahedron) is represented by dots. The green spheres denote the positions of the (3, -3) critical points (CPs) along the S-S lines, the red spheres are referred to the (3, -1) CPs and, finally, the violet sphere shown inside the triangular section (right side of the c) panel) represents the position of the (3, -3) CP belonging to the S-center line.

tion data predict a stronger S-S interlayer interaction than DFT. Moreover, the experimental ED is characterized by 3 maxima in the direction of the 3 neighboring, symmetry-related S atoms, while the theoretical one exhibits only one maximum directed towards the center of the S-atom tetrahedron (see Figure 1), suggesting that the theoretical DFT description of the interlayer interactions indeed qualitatively differs from the experimental one. In order to investigate the reasons of this discrepancy, we analyze the results of our DFT calculations and focus on the two directions of main interest, namely the S-center and the S-S line. Using the Bader nomenclature, for each line we characterize the (3, -3) critical point (CP) evaluating the position, \mathbf{r}_{max} , where the charge density reaches its maximum value, the density at this point, $n(\mathbf{r}_{max})$, and the Laplacian, $\nabla^2 n(\mathbf{r}_{max})$. Furthermore, we do the same for the (3, -1) CP, computing \mathbf{r}_{min} , $n(\mathbf{r}_{min})$, and $\nabla^2 n(\mathbf{r}_{min})$. As a preliminary analysis, we have

computed the ED and the Laplacian along the Ti-S line, identifying the main features of the polar covalent bond in the intralayer plane. The values that characterize the ED are reported in Table S1 of *Supporting information*. Two non-equivalent (3, -3) CPs are found along the Ti-S line (see top left panel in Figure S1 of *Supporting information*). The (3, -1) CP is instead located at 1.12 Å from the Ti atom. As can be seen, looking at Table S1 of *Supporting information*, very similar values are predicted by all the DFT functionals applied and most of these are also in good agreement with the experimental data.

A similar analysis can be also applied to characterize the interlayer bonding: the properties of the (3, -3) CP for both the S-S and S-center lines, and for the (3, -1) CP along the the S-S line are summarized in Table 1 and 2, respectively. In the interesting case of the S-S line, the PBE, rVV10, and rVV10($b=10.0$) functionals predict a maximum value of the ED at a distance $\mathbf{r}_{max} \sim 0.61$ Å from the reference S atom, with a relative error of ~ 13 % with respect to the experimental result,¹⁴ while the error is slightly larger with rVV10($b=1.0$) and LDA functionals.

Table 1: Properties at the (3, -3) CP along the S-S and S-center lines, evaluated using different DFT functionals.

	line	\mathbf{r}_{max} (Å)	$n(\mathbf{r}_{max})$ ($e/\text{Å}^3$)	$\nabla^2 n(\mathbf{r}_{max})$ ($e/\text{Å}^5$)
rVV10	S - S	0.614	1.102	-9.163
	S - center	0.614	1.132	-10.052
rVV10($b=1.0$)	S - S	0.607	1.050	-8.663
	S - center	0.605	1.081	-9.479
rVV10($b=10.0$)	S - S	0.614	1.105	-9.222
	S - center	0.614	1.132	-9.985
PBE	S - S	0.614	1.095	-9.093
	S - center	0.614	1.129	-9.934
LDA	S - S	0.579	1.141	-10.016
	S - center	0.579	1.172	-11.419
rVV10 _{opt}	S - S	0.609	1.074	-8.950
	S - center	0.607	1.102	-9.766
Experiment ¹⁴	S - S	0.707	1.150	-9.460
Theory ¹⁴ (SCAN+rVV10)	S - center	0.711	1.080	-8.910

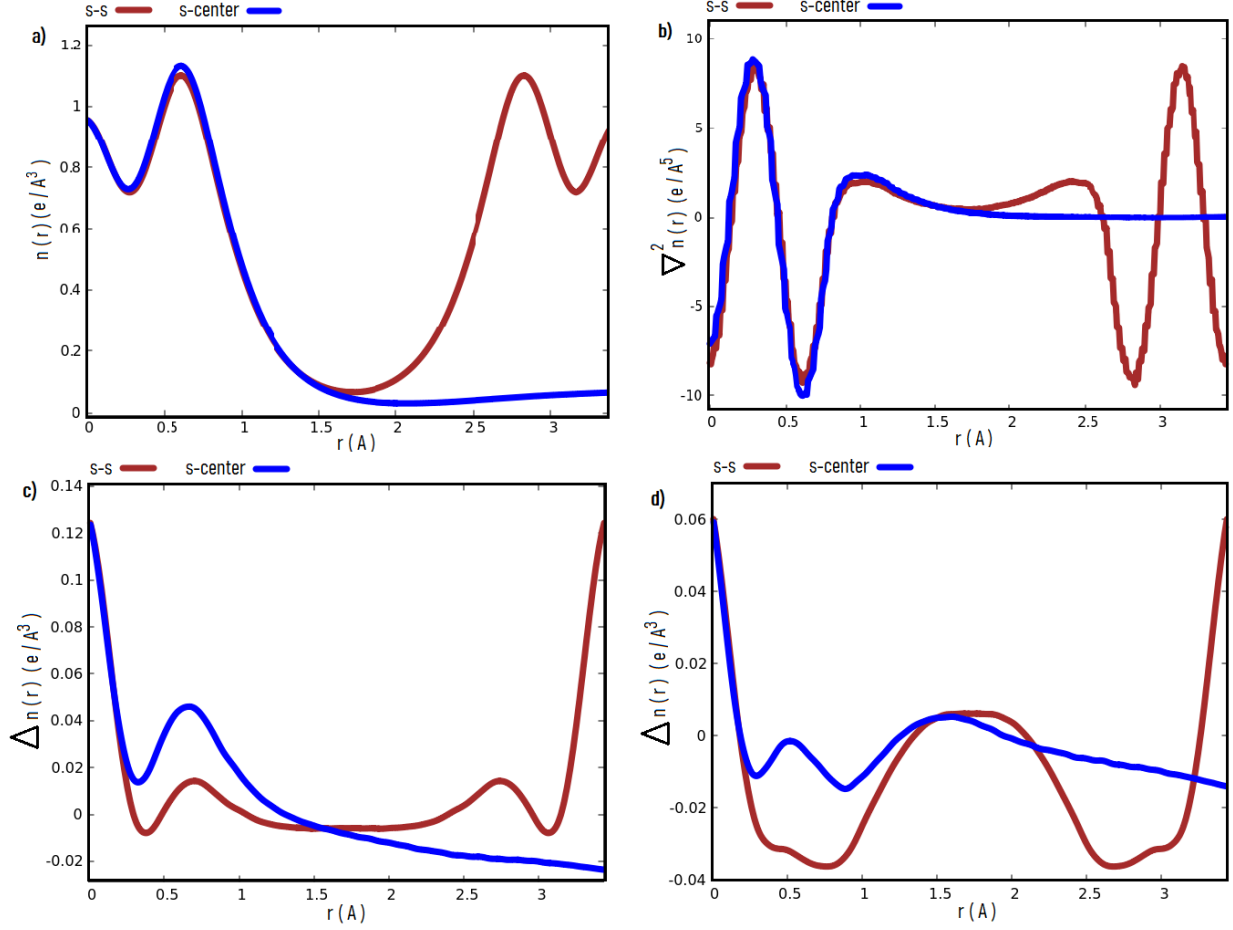


Figure 2: a) ED computed along the S-S and S-center line with the PBE functional. b) Corresponding Laplacian profiles. The small oscillations of the Laplacian profile are due to the finite-size of the real space mesh considered for the ED computation. In this case $\nabla^2 n(\mathbf{r}_{max})$ and $\nabla^2 n(\mathbf{r}_{min})$ are estimated by a parabolic interpolation $f(r \sim c) = c_2(r-c)^2 + k$, where the expansion center is $c = \mathbf{r}_{max}$ or $c = \mathbf{r}_{min}$. c) ED deformation $\Delta n(\mathbf{r})$ computed using the PBE functional and d) the rVV10($b=1.0$) functional. Curves obtained by rVV10 and rVV10($b=10.0$) functionals are very similar to the PBE ones and therefore are not reported.

The $n(\mathbf{r}_{max})$ values are all very similar and in reasonable agreement with the experimental data, with the LDA functional that shows the best agreement with the experimental value. The rVV10($b=1.0$) result, for which the maximum discrepancy occurs, has a deviation of only $\sim 9\%$. The Laplacians $\nabla^2 n(\mathbf{r}_{max})$ are also in acceptable agreement with the experimental values. Again, the result of the rVV10($b=1.0$) functional exhibits the maximum deviation from the experiment, with a discrepancy of $\sim 8\%$. This means that, at a distance r_{max} from the reference S atom, along the S-S line, with rVV10($b=1.0$), the ED deformation is slightly smaller than for the other functionals.

For the S-center line a direct comparison with experimental data is not available, so we take as reference the theoretical SCAN+rVV10 result reported by Kasai *et al.*¹⁴ The S-center line is characterized by the same \mathbf{r}_{max} value found for the S-S line, again with a small deviation of the value obtained with rVV10($b=1.0$) and LDA. Even in this case, the results for the ED and the Laplacians are in line with the theoretical reference data.¹⁴ Interestingly, for each functional employed, a slightly larger $n(\mathbf{r}_{max})$ value than that relative to the S-S line is observed, with a stronger ED deformation described by the associated Laplacian, indicating that the charge deformation along the S-center line is stronger than for the S-S line. The maximum deviation from the reference values, for both ED and Laplacians, occurs again for the LDA functional with an error of $\sim 8\%$ and $\sim 28\%$, respectively.

Table 2: Properties at the (3, -1) CP along the S - S line, evaluated using different DFT functionals. The theoretical (SCAN+rVV10) result reported, is the result achieved after a multipolar refinement of the pure DFT density (see ref. 14 for details).

	\mathbf{r}_{min} (Å)	$n(\mathbf{r}_{min})$ (e/Å ³)	$\nabla^2 n(\mathbf{r}_{min})$ (e/Å ⁵)
rVV10	1.718	0.068	0.486
rVV10($b=1.0$)	1.718	0.079	0.461
rVV10($b=10.0$)	1.718	0.067	0.481
PBE	1.718	0.067	0.460
LDA	1.718	0.070	0.468
rVV10 opt	1.718	0.074	0.464
Theory ¹⁴ (SCAN+rVV10)		0.058	0.727
Experiment ¹⁴		0.086	0.691

The S-S bond shows a symmetric ED distribution along the line connecting the two S atoms (see Figure 2a)), with \mathbf{r}_{min} exactly halfway between the two S atoms. Our computed $n(\mathbf{r}_{min})$ values, with the PBE, rVV10, and rVV10($b=10.0$) functionals, as well as LDA, are in very good agreement with the DFT densities presented in ref. 14, exhibiting a significant underestimate (by about 22 %) of the ED at the interlayer BCP, with respect to the experimental value. Interestingly, using the rVV10($b=1.0$) functional, the discrepancy with the experiment is instead considerably reduced to about 8 %. Note that the reported, theoretical SCAN+rVV10 value,¹⁴ is slightly below (and therefore slightly worse than) all our results. For the (3, -1) CP, the Laplacian sign is always positive, as expected, indicating that the interlayer BCP located at \mathbf{r}_{min} is a point where a charge depletion occurs. In Figure 2a) and 2b), an example of ED profiles and Laplacians, at the PBE level, along the S-S and S-center lines are shown, while in the bottom part, a comparison between the PBE ED deformation $\Delta n(\mathbf{r})$ (Figure 2c)) and that obtained by rVV10($b=1.0$) (Figure 2d)) is made along the same lines, highlighting that rVV10($b=1.0$) predicts a stronger charge depletion in the vicinity of the reference S atom than PBE and the other functionals. A consequent charge accumulation in the interlayer region appears, as confirmed by the higher ED $n(\mathbf{r}_{min})_{S-S}$ at the (3, -1) CP accompanied by a smaller Laplacian value $\nabla^2 n(\mathbf{r}_{min})_{S-S}$ (see Table 2) that indicates a slightly less charge depletion than for the other functionals considered.

The ED deformation map in the interlayer plane, presented in Figure 3, is very similar with the PBE, rVV10, and rVV10($b=10.0$) functionals (as well as the LDA case which it is not reported), while the same is not true for rVV10($b=1.0$), which predicts a more pronounced ED deformation in the region between the two S atoms belonging to adjacent layers. The Laplacian map of the interlayer plane is presented in Figure S2 of the *Supporting information*: in this case, no significant differences for the functional schemes adopted up to now are found, as well as for LDA and the other schemes presented below.

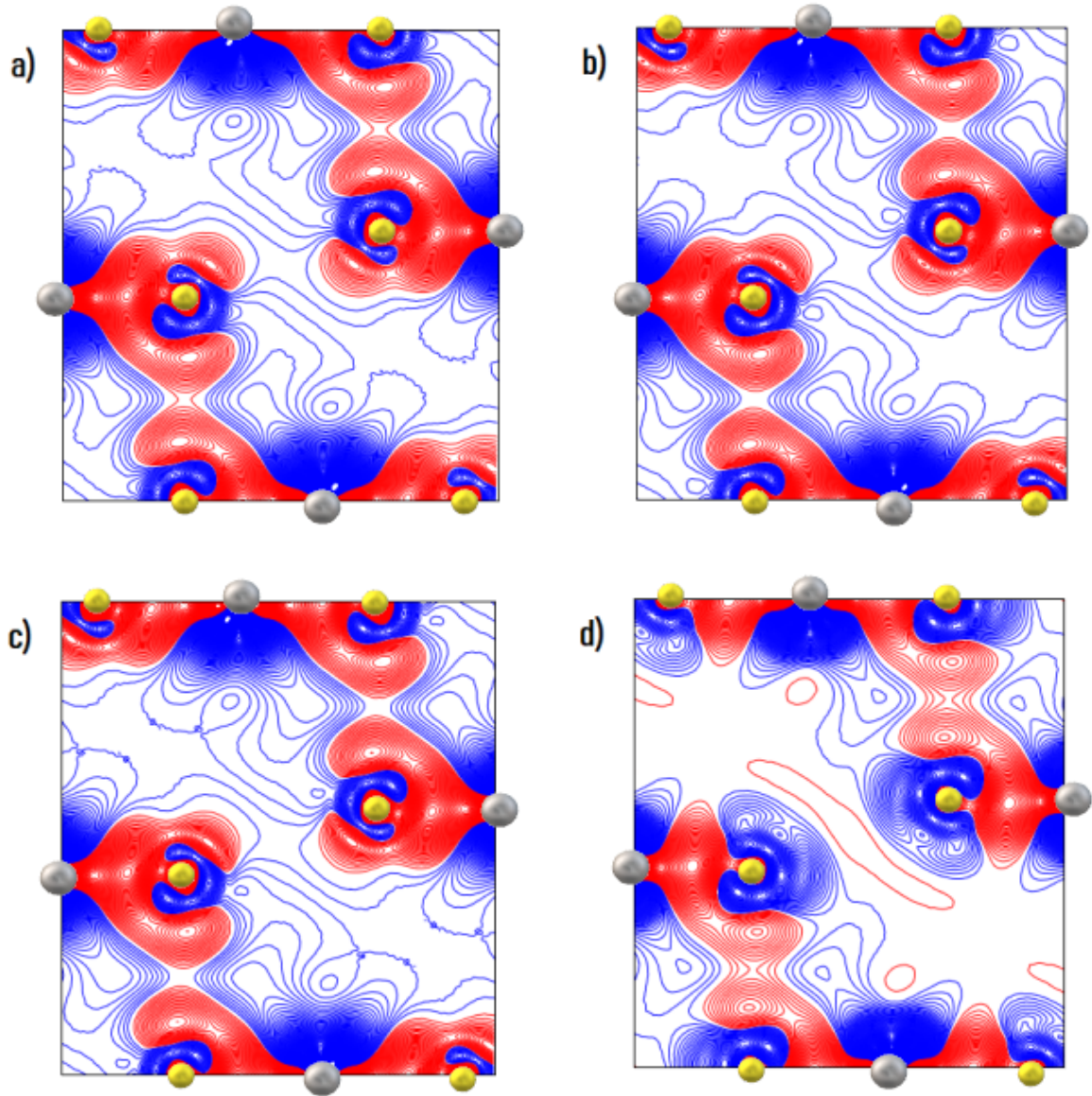


Figure 3: ED deformation map in the interlayer plane using four different functionals: a) PBE, b) rVV10, c) rVV10($b=10.0$), and d) rVV10($b=1.0$). The Ti atom are represented by grey spheres, while the S atoms are the yellow spheres. In the present maps, the smallest isoline value reported is $0.001 \text{ e}/\text{\AA}^3$, with red and blue contours that represent charge accumulation and depletion, respectively.

Table 3: Cohesive energy (CE) and interlayer binding energy (ILBE), see text for the definitions, obtained using the experimental lattice parameter c (first and second column) and the corresponding quantities (denoted by the * symbol, in the fourth and fifth column) relative to the c value (third column) optimized for each adopted functional. The reported reference CE and c values are experimental data, while, for the ILBE, we provide theoretical RPA³⁴ and MBD estimates. The quantity V , in the sixth column, represents the total charge belonging to the atomic basin A , surrounding the S atom. The charge q_A , contained in A , and the atomic dipole moment of the S atom, $d(q_A)$, are reported in column seven and eight respectively.

	CE (eV)	ILBE (meV/Å ²)	c (Å)	CE* (eV)	ILBE* (meV/Å ²)	V (Å ³)	q_A (e)	$d(q_A)$ (eÅ)
rVV10	-15.602	-27.828	5.728	-15.603	-27.888	23.775	-0.860	0.380
rVV10($b=1.0$)	-27.928	-192.073	4.934	-42.140	-1613.663	23.781	-0.861	0.383
rVV10($b=10.0$)	-15.035	-16.609	5.878	-15.045	-17.698	23.574	-0.796	0.324
PBE	-15.150	-3.013	6.595	-15.189	-0.861	23.804	-0.871	0.404
LDA	-18.633	-17.275	5.470	-18.633	-18.357	23.648	0.829	0.383
rVV10 _{opt}	-25.889	-151.580	5.123	-25.310	-175.506	23.615	-0.809	0.373
Experiment	-14.805 ³⁵		5.665 ¹⁴	-14.805		23.470 ¹⁴	-0.820 ¹⁴	0.030 ¹⁴
Theory (RPA)		-18.900 ³⁴			-18.900	23.630 ¹⁴	-0.800 ¹⁴	0.340 ¹⁴
Theory (MBD)		-19.031			-19.031			

A summary of the basic energetic quantities of TiS₂ and the atomic properties of the reference S atom is reported in Table 3. We optimized the interlayer lattice constant c for each functional adopted (third column of Table 3), obtaining results close to the experimental reference value using the rVV10 and rVV10($b=10.0$) functionals, with an error of only ~ 3 %. Instead, the quality of the PBE, rVV10($b=1.0$), and LDA estimates is worse, with PBE that substantially overestimates, and LDA and rVV10($b=10.0$) which instead underestimate. This behavior does not come as a surprise: in fact LDA and the semilocal PBE functional are not able to properly describe the vdW interactions, while the rVV10($b=1.0$) functional was deliberately built to artificially increase the strength of short-range vdW interactions, thus leading to a larger interlayer bonding energy and to a shorter layer-layer distance. The atomic cohesion energy (CE) is defined as $E(\text{TiS}_2) - E(\text{Ti}) - 2E(\text{S})$, where $E(\text{TiS}_2)$ is the total energy of the TiS₂ systems, while $E(\text{Ti})$ and $E(\text{S})$ are the total energies of the isolated T and S atoms. This quantity mainly reflects the intensity of the strong, intralayer Ti-S covalent bonds. Considering both the experimental configuration (first column) and the one in which the lattice constant c is optimized (fifth column), quite similar results are achieved using PBE, rVV10, and rVV10($b=10.0$), with an average discrepancy with the experimental reference value of ~ 5 %. However, the CE value obtained with the rVV10($b=1.0$) functional is largely overestimated implying that artificially increasing the strength of the

short-range vdW interaction leads to a severe overbinding even of the Ti-S covalent bond. Therefore, the improvement in the ED distribution using rVV10($b=1.0$) comes at the expense of an unacceptable deterioration in the description of the energetic properties. This is also confirmed by the analysis of the interlayer binding energy (ILBE), defined as $E(\text{TiS}_2) - E(\text{TiS}_2)_{c/a=5}$, representing the interaction energy between two adjacent layers of the material. Here, $E(\text{TiS}_2)_{c/a=5}$ indicates the total energy of the system when the c parameter is set to $5a \sim 17 \text{ \AA}$, which corresponds to a distance so large that the interlayer interaction is negligible. In order to have a more sound comparison with reference values, in addition to the RPA value reported in the literature,³⁴ we have also computed the ILBE using the Many-Body Dispersion (MBD) approach³⁶ which allows for an effective RPA description of long-ranged vdW interactions, beyond conventional pairwise approximations. Within MBD one maps the atomic response functions into a set of quantum harmonic oscillators, mutually coupled at the dipole-dipole level. Due to the inclusion of many-body effects, MBD can reach chemical accuracy for a broad variety of systems (from small molecules to large nanostructure and periodic materials).³⁶ In particular, many-body effects were shown to be crucial in two-dimensional vdW materials,³⁷ as they can qualitatively alter the power law scaling of dispersion interactions. Remarkably (see Table 3) the MBD estimate is very close to the RPA value reported in ref. 34.

As expected, PBE dramatically underestimates the ILBE (the discrepancy is even worse considering the optimal configuration predicted by PBE), a behavior that can be clearly ascribed to the inadequate inclusion of vdW effects by PBE. As can be seen in Table 3, the standard rVV10 functional significantly overestimates the ILBE, while rVV10($b=10.0$) gives a result reasonably close to the reference values. Interestingly, the LDA estimation is very good, showing the best agreement with the reference values. However, one must point out that this good performance is accidental: the well-known LDA overbinding due to the overestimate of the long-range part of the exchange contribution, somehow mimics the missing vdW interactions, thus leading to reasonable estimates of the binding energies

in a wide range of systems.³⁸ Instead, similarly to what observed for the CE, rVV10($b=1.0$) predicts a very large, unphysical ILBE.

Looking at Table 3 our computed atomic basin volume V turns out to be in good agreement with the theoretical and experimental reference values, and the same is true for the total charge q_A contained in the atomic basin, with all the adopted functionals that predict quite similar values (which the partial exception of rVV10($b=10.0$) which gives a significantly less negative accumulated charge). The negative value of q_A is consistent with the higher electronegativity of the S atom, which therefore behaves as the electron-acceptor in the polar covalent Ti-S bond. The values of the dipole moment of the S atom, $d(q_A)$, computed through the spherical multipolar expansion (see section II), are, for all the considered functionals, in line with the theoretical reference data but much larger than the experimental estimate, thus reproducing the discrepancy between theory and experiment discussed above. In more detail, PBE exhibits the largest discrepancy, thus confirming that this functional is not adequate, while the rVV10($b=10.0$) functional gives a slightly less pronounced dipole moment, suggesting a description a little closer to the experiment, although even the rVV10($b=10.0$) value of $d(q_A)$ is still quite far from the experimental one.

So far, our results for the ED distribution, and for the energetic and atomic properties of TiS_2 , are in line with the conclusions of Kasai *et al.*¹⁴ concerning the theoretical DFT description. In particular, our analysis of CPs (see Table 1), confirms that the ED predicted at DFT level along the S-S line is smaller than the one along the S-center line, at variance with the experimental evidence. Small, quantitative differences between our calculations and the theoretical SCAN+rVV10 results reported by Kasai *et al.*¹⁴ can be easily explained by the different DFT functional adopted and by other technical differences: for example, in ref. 14 a finer mesh of $22 \times 22 \times 13$ k-points was used for the sampling of the BZ, this choice being motivated by the need of describing core electron oscillations to carry out a multipole refinement procedure.¹⁴

Coming to a more detailed analysis, we observe (see Figure S2 and Figure S3 of *Supporting*

information) that the maps of $\Delta n(\mathbf{r})$ and $\nabla^2 n(\mathbf{r})$ obtained by rVV10($b=10.0$) are very similar to those given by the standard rVV10 functional and also by PBE, thus suggesting that the interlayer ED distribution is weakly affected by an augmented damping applied to the short-range vdW interactions; this is also quantitatively confirmed by the the values of $n(\mathbf{r})$ and $\nabla^2 n(\mathbf{r}_{max})$ evaluated at the (3, -3) CP (see Table 1). A small difference can be noticed only at the (3, -1) CP, where the rVV10($b=10.0$) value of $\nabla^2 n(\mathbf{r}_{max})$ almost coincides with that obtained by the standard rVV10 result but weakly differs from the PBE one. The situation is different considering rVV10($b=1.0$), namely a functional where the short-range vdW interaction is artificially increased; in fact, although the ED and the Laplacian at the CPs defined above are similar to the same quantity evaluated by the other functionals, more pronounced differences can be observed away from the BCP, reflecting an accumulation of the ED in the interlayer region. As a consequence, rVV10($b=1.0$) predicts an ILBE value which appears to be dramatically overestimated. Moreover, with rVV10($b=1.0$) one can observe (Figure 3d)) a considerable ED deformation between the reference S atom and the other S atom belonging to the same layer, thus indicating a strong intralayer S-S interaction, a feature not observed with the other functionals and absent in the experimental description.

To overcome (at least partially) these evident shortcomings of rVV10($b=1.0$), we have also tested another DFT functional, rVV10($b=1.1, C=0.00207$), named as rVV10*opt*, which is characterized by a new C parameter, thus modifying the value of the effective C_6 coefficient responsible for the long-range behavior of the vdW interactions, and also by a slightly changed b parameter. The ED deformation map obtained with this new functional is shown in Figure 4. As can be seen, by artificially manipulating the long-range component of vdW interactions, the unphysical ED accumulation in the intralayer S-S region disappears and, more interestingly, a small tendency to form a localized S-S interlayer bond can be observed, although the intensity of the interlayer ED deformation is again underestimated, being 7 times smaller than the experimental one.¹⁴ rVV10*opt* preserves the nature of the S-Ti intralayer bond and the basic properties of the ED at the two non equivalent (3, -3) CPs

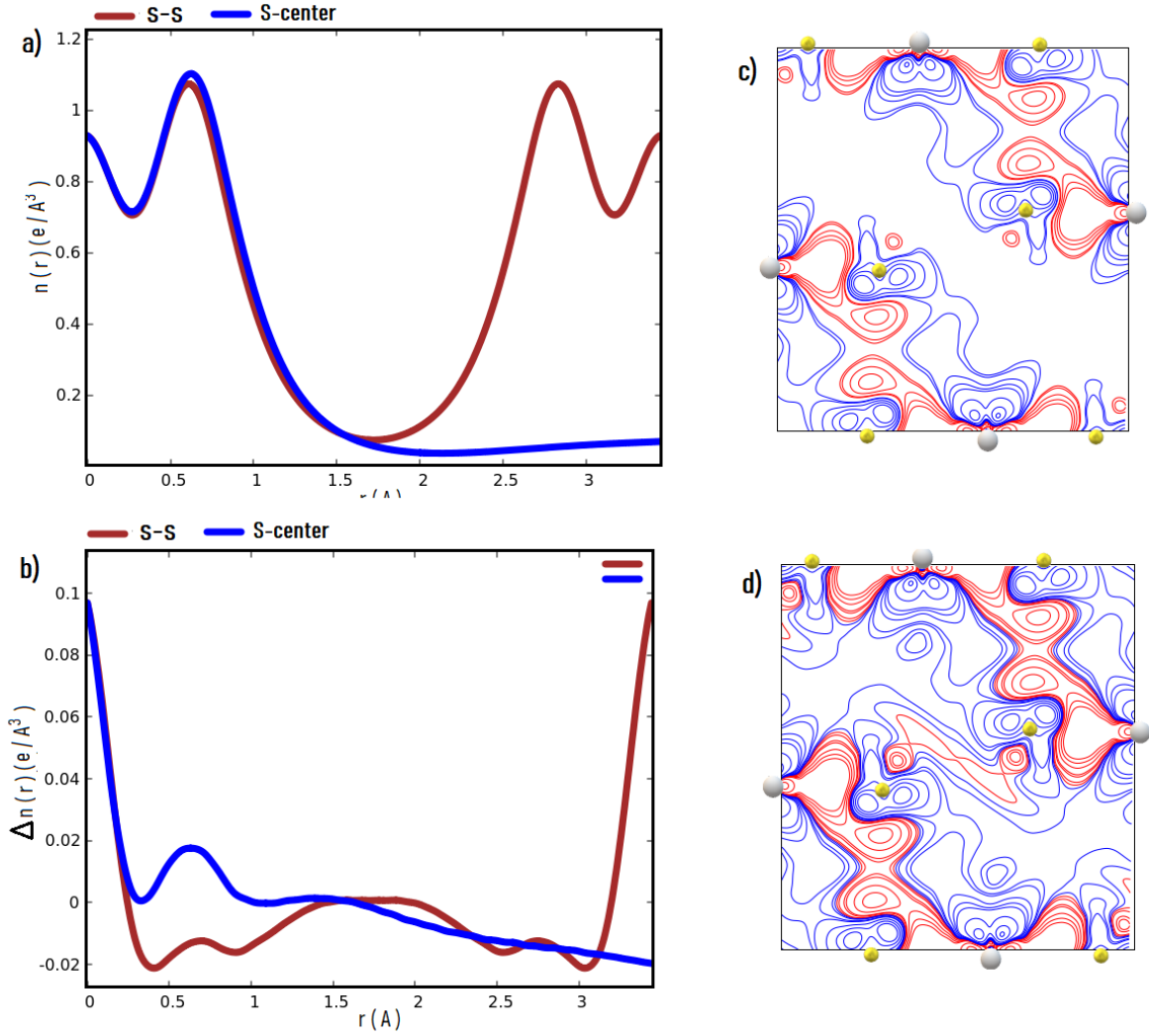


Figure 4: a) ED along the S-S and S-center line, obtained using the *rVV10opt* functional. b) Associated ED deformation $\Delta n(\mathbf{r})$. c) ED deformation map in the Ti-S intralayer plane. d) ED deformation map in the interlayer plane with a contour of $\pm 0.01 e/\text{\AA}^3$. e) ED deformation map in the interlayer plane with a smaller contour of $\pm 0.001 e/\text{\AA}^3$.

and at the (3, -1) CP; in fact the positions of these points are unchanged and the ED and Laplacian values, reported in Table 1 are in line with the other functionals employed. Similar conclusions hold considering the S-S and S-center lines. Finally, one must point out that, even with this new functional, the ED accumulation along the S-S line is predicted to be smaller than along the S-center line, differently from the experimental findings. Therefore, considering that (see Table 3) $rVV10_{opt}$ still largely overestimate the ILBE, although it slightly reduces the dramatic overbinding of $rVV10(b=1.0)$, one can conclude that it is not possible to achieve, at the same time, a description of energetic and ED deformation features, in reasonable agreement with the experimental results, by simply tuning the values of the b and C parameters of the $rVV10$ functional, which determine the strength of short/medium- and long-range vdW effects.

As an alternative strategy to reduce the discrepancy between the theoretical DFT description of TiS_2 and the experimental evidence, we have also investigated the effect of introducing a modified pseudopotential for S. The S atom is characterized by the $[Ne]3s^23p^4$ ground-state configuration, so that in neutral S atom d orbitals are empty, and, in simple molecules, they are nearly unpopulated. Nonetheless, it was shown¹⁷ that they can play a significant role: for instance, even in the small S_2 molecule an appreciable improvement in the binding-energy estimate was observed by adopting for S a pseudopotential built by taking into account d orbitals, which are expected¹⁷ to give S enhanced polarizability and enable a great variety of bonding configurations through hybridization. In fact, although some orbitals (for instance, in this case the d ones) are not bound states of the neutral atom, it is necessary¹⁷ to choose a partially ionized atomic reference configuration, with a charge slightly different from the neutral atom, to get pseudopotentials that are better tailored for applications to solid-state and extended systems, since the effective configuration of these systems differs from that of the neutral atom.

Following this approach, we have generated a novel S ultra-soft pseudopotential, based on the configuration $[Ne]3s^23p^{3.0}3d^{1.0}$, using the Troullier-Martins pseudization method³⁹ with

non-linear core corrections.⁴⁰ Coupling it with the rVV10 functional, we have developed the rVV10*d* scheme.

First we have applied the rVV10*d* functional to the simple case of the S₂ molecule, which is in itself an interesting system, being an ubiquitous intermediate in the combustion, atmosphere, and interstellar space.⁴¹ With rVV10*d*, while the equilibrium distance is unchanged with respect to rVV10, we obtain a substantial improvement of the molecular binding-energy and a slight improvement of the vibrational frequency (see table S3 of *Supporting information*), thus confirming the importance of including the *d* orbitals in such a system. In particular, considering the binding energy, the more than 20 % discrepancy with the experimental reference value of the rVV10 original functional, reduces to only about 3 % with rVV10*d*. We have therefore recomputed the energetic and electronic properties of TiS₂ using the new rVV10*d* functional.

Table 4: Properties at the (3, -3) CPs along both the S-S and S-center line and at the (3, -1) CP on the S-S line, computed using rVV10*d* and compared with the results achieved with rVV10.

(3, -3) CPs	line	\mathbf{r}_{max} (Å)	$n(\mathbf{r}_{max})$ (e/Å ³)	$\nabla^2 n(\mathbf{r}_{max})$ (e/Å ⁵)
	rVV10	S - S	0.614	1.102
	S - center	0.614	1.132	-10.052
rVV10 <i>d</i>	S - S	0.643	1.094	-9.253
	S - center	0.643	1.126	-9.990
Experiment ¹⁴	S - S	0.707	1.150	-9.460
Theory ¹⁴ (SCAN+rVV10)	S - center	0.711	1.080	-8.910
(3, -1) CP	line	\mathbf{r}_{min} (Å)	$n(\mathbf{r}_{min})$ (e/Å ³)	$\nabla^2 n(\mathbf{r}_{min})$ (e/Å ⁵)
	rVV10	S - S	1.718	0.068
rVV10 <i>d</i>	S - S	1.718	0.068	0.482
Experiment ¹⁴	S - S		0.086	0.691
Theory ¹⁴ (SCAN+rVV10)	S - S		0.058	0.727

As can be seen in Table 4, at the (3, -3) and (3, -1) CPs, with rVV10*d*, the basic ED properties are very similar to those obtained by the standard rVV10 functional. However, the effect of replacing rVV10 with rVV10*d* is evident looking at Figure 5: one can appreci-

ate a significant ED accumulation along the S-S line, which is not present using the other DFT functionals considered, including that (SCAN+rVV10) adopted by Kasai *et al.*¹⁴ Although the discrepancy with the experimental description is only partially resolved (even with rVV10*d* the ED accumulation along the S-S line is predicted to be slightly smaller than along the S-center line), a clear improvement is evident, which we attribute to the increased flexibility of the new S pseudopotentials that is able to better reproduce the variety of bonding structures and hybridization processes involving S atoms.

Table 5: Energetic and structural properties of TiS₂, together with the atomic basin properties of the S atom, obtained with the rVV10*d* and compared with rVV10. The notation used is the same as in Table 3.

	CE (eV)	ILBE (meV/Å ²)	<i>c</i> (Å)	CE* (eV)	ILBE* (meV/Å ²)	V (Å ³)	q _A (e)	d(q _A) (eÅ)
rVV10	-15.602	-27.828	5.728	-15.603	-27.888	23.775	-0.860	0.380
rVV10 <i>d</i>	-15.640	-20.888	5.809	-15.646	-20.771	23.761	-0.860	0.390
Experiment	-14.805 ³⁵		5.665 ¹⁴	-14.805		23.470 ¹⁴	-0.820 ¹⁴	0.030 ¹⁴
Theory (RPA)		-18.900 ³⁴			-18.900	23.630 ¹⁴	-0.800 ¹⁴	0.340 ¹⁴
Theory (MBD)		-19.031			-19.031			

Remarkably, with rVV10*d*, an even more substantial improvement in energetic properties takes place. In fact, while the CE remains very close to that obtained by rVV10, suggesting that *d* orbitals of S do not play a significant role in the formation of strong, intralayer covalent bonds, the change in the ILBE is instead considerable: assuming the experimental structure, our computed ILBE differs by only ~ 2 meV/Å² from the theoretical references, i.e. high quality, RPA,³⁴ and MBD estimates, which represents a relative error of about 10 %; such an error is comparable to that obtained by the much more expensive meta-GGA approaches and is much smaller than that (about 47 %) found with the original rVV10 functional which clearly overbinds. As can be seen in Table 5, the good energetic description of rVV10*d* is preserved even considering a TiS₂ configuration where the experimental lattice constant *c* is replaced by the *c* value optimized with rVV10*d* (whose prediction is only slightly worse than the rVV10 one), thus increasing the confidence in the reliability of this functional.

As far as the dipole moment is concerned, with rVV10*d* this quantity is not improved with respect to the experimental estimate (see Table 5), which can be rationalized as fol-

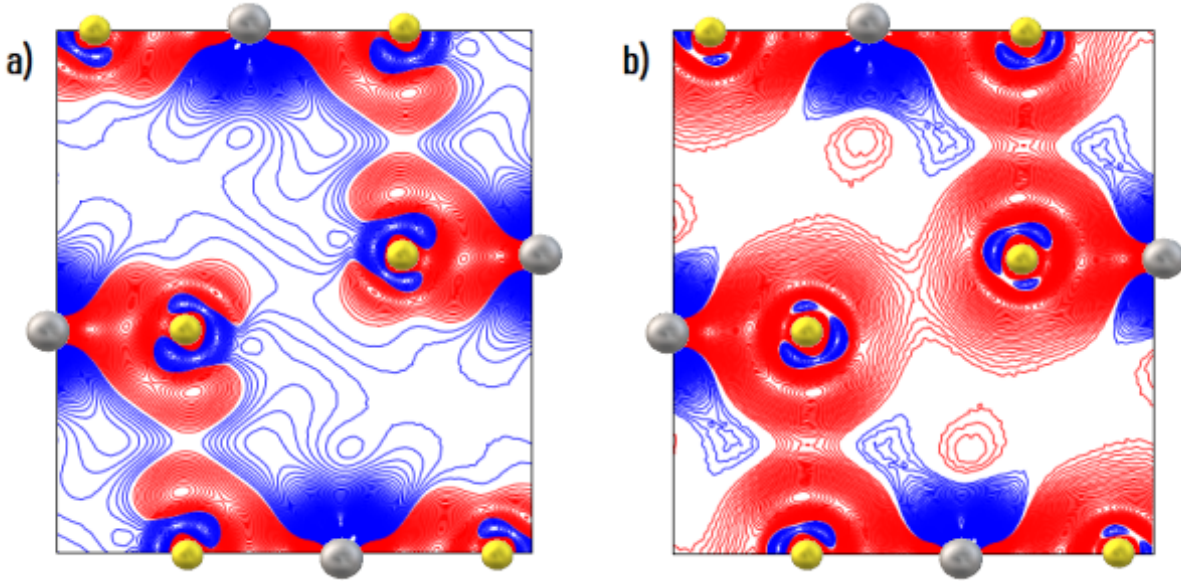


Figure 5: Comparison between the ED deformation obtained by the standard rVV10 functional (panel a) and rVV10d (panel b). The smallest isoline value reported is $0.001 \text{ e}/\text{\AA}^3$, with red and blue contours that represent charge accumulation and depletion, respectively.

Table 6: Optimized lattice constant c , ILBE and ILBE* computed for TiS_2 and three other TMDs, employing both rVV10 and rVV10d functionals. The last two lines report the mean error (ME) and the mean absolute relative error (MARE).

	rVV10d			rVV10		
	ILBE ($\text{meV}/\text{\AA}^2$)	c (\AA)	ILBE* ($\text{meV}/\text{\AA}^2$)	ILBE ($\text{meV}/\text{\AA}^2$)	c (\AA)	ILBE* ($\text{meV}/\text{\AA}^2$)
TiS_2	-20.771	5.809	-20.888	-27.828	5.728	-27.888
ref. 34	-18.900	5.665	-18.900	-18.900	5.665	-18.900
MoS_2	-20.296	12.810	-22.147	-29.242	12.530	-29.683
ref. 34	-20.530	12.300	-20.530	-20.530	12.300	-20.530
TaS_2	-18.924	6.152	-19.344	-29.367	6.009	-29.369
ref. 34	-17.680	5.900	-17.680	-17.680	5.900	-17.680
HfS_2	-18.391	5.938	-18.530	-23.452	5.858	-23.603
ref. 34	-16.130	5.840	-16.130	-16.130	5.840	-16.130
ME	-1.285	0.251	-1.917	-9.162	0.105	-9.362
MARE (%)	7.5	3.2	10.7	50.3	1.3	51.1

lows: as a consequence of applying the modified rVV10d functional, the electronic charge is more widespread around the S atoms, which leads to a better agreement with experimental ED findings and to an improved estimate of the ILBE. However this increased charge delocalization does not occur exclusively in the interlayer region, but also, for instance, in the intralayer region, particularly along lines connecting neighboring S atoms. Therefore,

the net delocalization effect (see Figure 5) is approximately isotropic so that the S dipole moment is not appreciably changed from that estimated by the original rVV10 functional.

We have also performed additional calculations on TiS₂ by adopting vdW-corrected DFT functionals different from rVV10. Interestingly, while the inclusion of the new pseudopotential involving *d* orbitals leads to improvements similar to those observed with rVV10 in the description of the ED profiles (with a small charge accumulation in the interlayer region) and in the ILBE estimate, using vdW-corrected DFT functionals based on non-local functionals, such as VDW-DF-cx,⁴² the same is not the case when vdW-corrected DFT functionals are adopted, which are more empirical in character (and not directly dependent on the detailed electron density distribution), such as the DFT-D3 approach,⁴³ which indicates that the new pseudopotential is indeed better suited to describe the subtle charge deformations occurring in this system. Finally, to further assess the validity of this novel approach, we have applied the rVV10*d* functional to other three different TMDs, whose chalcogen is always the S atom: MoS₂, TaS₂, and HfS₂. The results for the equilibrium lattice parameter *c*, as well as the ILBE and ILBE* (see Table 6), are very promising. The major flexibility of the new pseudopotential, embedded in rVV10*d* scheme, dramatically improves the energetic description of S-based TMDs, maintaining an appreciable quality of the estimate of the longitudinal lattice parameter *c*: in fact, although the error relative to *c* is $\sim 2\%$ bigger than with rVV10, the mean absolute relative error (MARE) of the ILBE is reduced by about *five* times; this means that the pronounced overbinding tendency of rVV10 is almost totally eliminated.

4 Conclusions

We have presented the results of a first principles, DFT investigation, of the energetic and electronic properties of TiS₂, that is a system where a puzzling discrepancy, between the distribution of the electron density obtained by X-ray diffraction data and that computed by state-of-the DFT schemes, has been recently reported, mainly concerning the interlayer

region between S atoms belonging to adjacent layers. We basically confirm this observation, using the LDA, the (semilocal GGA) PBE, the (vdW-corrected) rVV10 DFT functionals, and also a modified rVV10 functional (rVV10($b=10.0$)) where the b parameter has been increased so that short/medium-range vdW interactions are artificially damped. If instead the b parameter is considerably reduced to $b=1.0$ (rVV10($b=1.0$)) significant changes occur: a stronger ED deformation in the interlayer region is accompanied by a dramatic (and physically unrealistic) overestimate of the CE and ILBE terms. Substantially decreasing (by a 4.5 factor) the other (C) rVV10 parameter and further adjusting the b parameter (rVV10($b=1.1, C=0.00207$) functional) only slightly reduces the dramatic overbinding of rVV10($b=1.0$) scheme. Interestingly, a more substantial improvement, in the direction of making the theoretical description in closer agreement with the experiment, is obtained by adopting for S a modified, more flexible, pseudopotential, involving d orbitals (rVV10 d functional). Although the rVV10 d estimate of the atomic S dipole moment still remains substantially larger (see Table 5) than the experimental one, a consistent improvement in the description of the ED deformation in the interlayer region and of the ILBE is achieved. Probably, the residual discrepancy with the experiment could be only eliminated by an higher-level theoretical, first-principle approach, such as a Quantum Monte Carlo scheme, in principle able to include the whole set of correlation effects. Such an approach would be however extremely expensive computationally because very small ED deformations could only be accurately reproduced by very long simulations to get a sufficiently small statistical error associated to differential densities. In any case, although all fine details in the ED deformation map cannot be captured by rVV10 d , nonetheless we suggest that this DFT functional indeed represents a reasonable compromise between accuracy and efficiency for improving the theoretical description of TiS₂. Additional investigations indicate that similar improvements, particularly in the evaluation of energetic terms, can be obtained by DFT calculations based on the rVV10 d functional, applied also to other TMD materials containing S atoms and characterized by the same structure of TiS₂, such as TaS₂, HfS₂, and MoS₂.

5 Supporting information

6 Intralayer bonding

The analysis of the Ti-S covalent bond, which characterizes the intralayer interactions, is presented here. The electron density (ED) (panel a) and Laplacian (panel b) profiles computed along the Ti-S line, as well as the ED deformation (panel c) and the Laplacian map (panel d) of the Ti-S intralayer plane, are reported. Since the results achieved with all the functional schemes employed are very close to each other, we show only the PBE results as an example (Figure S1). In Table S1, the characterization of the two (3, -3) CPs and the (3, -1) CP is presented. As can be seen, very similar values are predicted by all the DFT functionals applied and these are also in good agreement with experimental data, with the exception of the LDA estimate of the Laplacian of (3, -3) CP #1, that exhibits a larger error and the Laplacian values at the (3, -1) CP, which are also substantially overestimated.

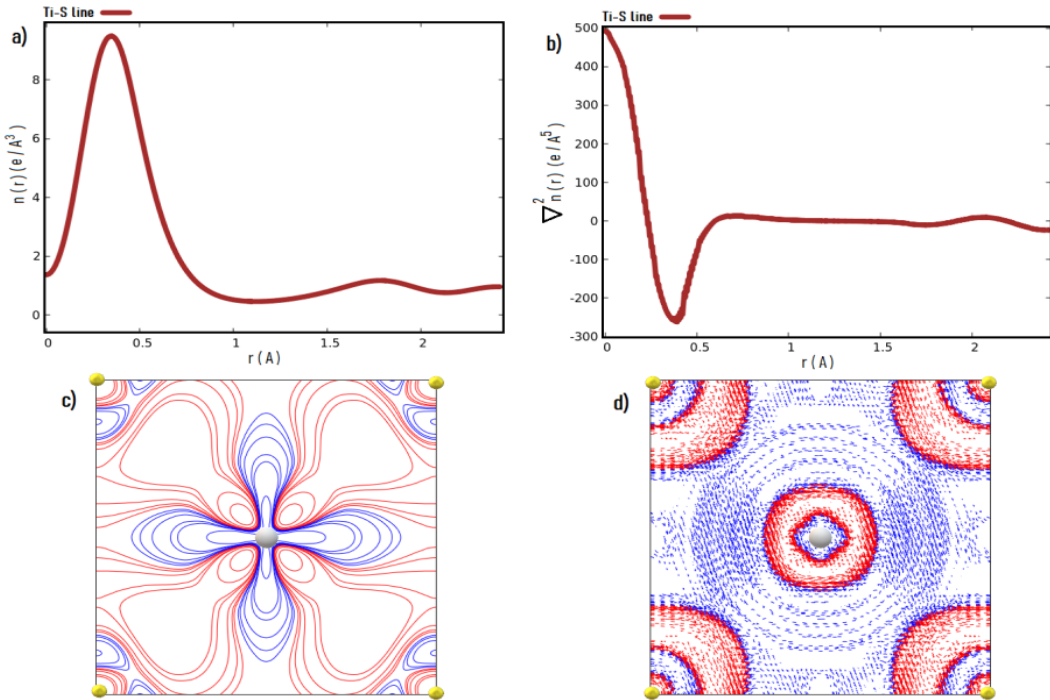


Figure 6: Ti-S intralayer bond. a) ED along the Ti-S line; local maxima denote the positions of the (3,-3) CPs, while the local minimum that of the (3,-1) one; b) Laplacian of the ED; c) ED deformation density map in the Ti-S plane; d) Laplacian map in the Ti-S plane. Here results obtained at the PBE level are reported as an example.

Table 7: Properties at the (3, -3) CPS and (3, -1) CP identified along the Ti-S line.

(3, -3) CP #1	\mathbf{r}_{max} (Å)	$n(\mathbf{r}_{max})$ (e/Å ³)	$\nabla^2 n(\mathbf{r}_{max})$ (e/Å ⁵)
rVV10	0.353	9.490	-253.367
rVV10($b=1.0$)	0.350	9.487	-251.214
rVV10($b=10.0$)	0.353	9.495	-252.613
PBE	0.352	9.497	-257.543
LDA	0.340	9.217	-221.444
rVV10 $_{opt}$	0.349	9.477	-255.304
Experiment ¹⁴	0.407	9.350	-253.000
Theory ¹⁴ (SCAN+rVV10)	0.407	9.310	-250.000
(3, -3) CP #2	\mathbf{r}_{max} (Å)	$n(\mathbf{r}_{max})$ (e/Å ³)	$\nabla^2 n(\mathbf{r}_{max})$ (e/Å ⁵)
rVV10	1.777	1.171	-10.315
rVV10($b=1.0$)	1.782	1.175	-9.978
rVV10($b=10.0$)	1.780	1.175	-10.789
PBE	1.781	1.172	-10.430
LDA	1.819	1.216	-10.091
rVV10 $_{opt}$	1.778	1.157	-10.165
Experiment ¹⁴	1.714	1.260	-11.300
Theory ¹⁴ (SCAN+rVV10)	1.707	1.200	-9.870
(3, -1) CP	\mathbf{r}_{min} (Å)	$n(\mathbf{r}_{min})$ (e/Å ³)	$\nabla^2 n(\mathbf{r}_{min})$ (e/Å ⁵)
rVV10	1.122	0.453	1.455
rVV10($b=1.0$)	1.126	0.448	1.211
rVV10($b=10.0$)	1.122	0.450	1.484
PBE	1.120	0.458	1.231
LDA	1.125	0.461	1.002
rVV10 $_{opt}$	1.124	0.453	1.245
Experiment ¹⁴		0.429	3.791
Theory ¹⁴ (SCAN+rVV10)		0.421	3.956

7 ED interlayer Laplacians

Here we present the Laplacian maps of the interlayer plane of interest, computed for all the functional employed (the LDA map is very similar to the ones shown).

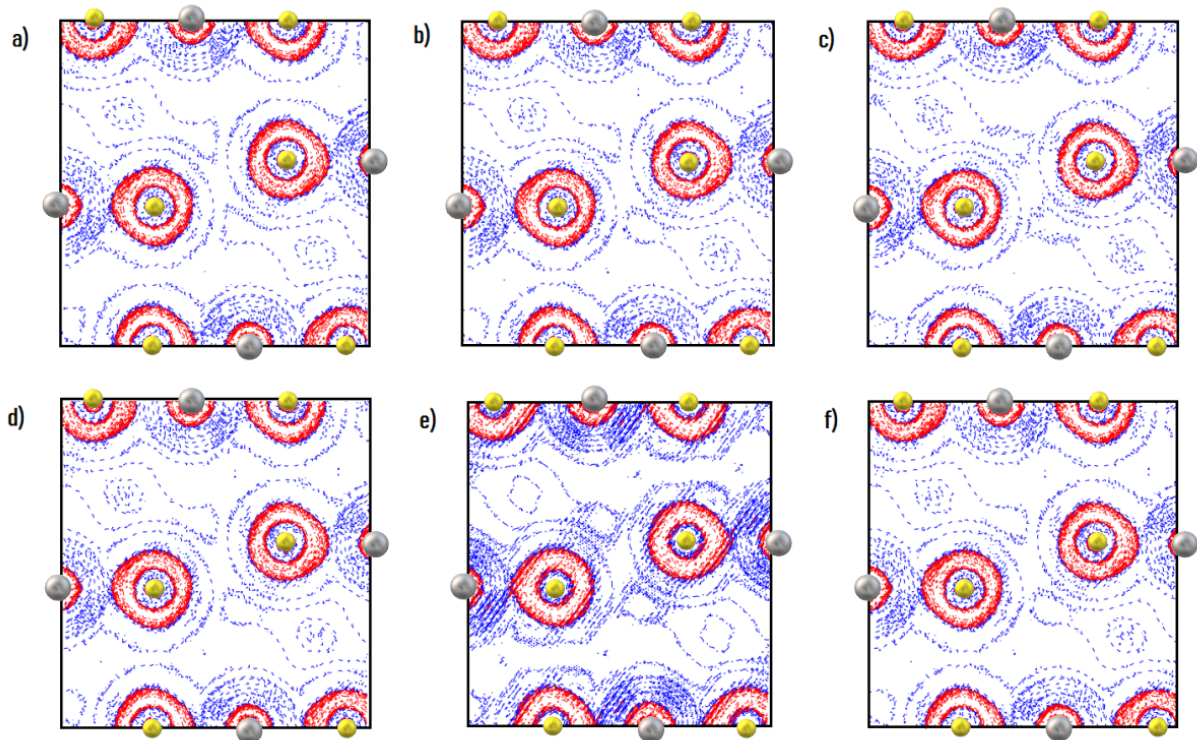


Figure 7: Laplacian map in the interlayer plane using different functionals: a) PBE, b) rVV10, c) rVV10($b=1.0$), d) rVV10($b=10.0$), e) rVV10 $_{opt}$, and f) rVV10 $_d$. The Ti atoms are represented by grey spheres, while the S atoms are the yellow spheres. The results are reported by using Bader contour lines of $[1, 2, 4, 8] \times 10^{[-3, -2, -1, 0, 1]} e/\text{\AA}^5$. In these maps red (blue) contours are associated to negative (positive) Laplacian values, which represents charge accumulation (depletion).

8 S₂ molecule characterization

The calculations for the S₂ molecule, were carried out using the same approach adopted for the simulations of the TiS₂ system (see section 2 in the main text); the only differences were the chosen supercell (a cube with sides of 13.2 Å) and the sampling of the BZ limited to the Γ point. Calculations were spin-polarized and the S₂ vibrational frequency was computed using the *PHonon* program of QE.

Table 8: Equilibrium distance (d), binding energy, and vibrational frequency of the S₂ molecule, computed with the rVV10 and rVV10*d* functionals.

	d (Å)	binding energy (eV)	vibrational frequency (cm ⁻¹)
rVV10	1.91	5.73	689
rVV10 <i>d</i>	1.91	4.57	692
Experiment	1.89 ¹⁷	4.74 ¹⁷	714 ± 12 ⁴¹

9 Acknowledgements

We acknowledge funding from Fondazione Cariparo, Progetti di Eccellenza 2017, relative to the project: "Engineering van der Waals Interactions: Innovative paradigm for the control of Nanoscale Phenomena".

References

- (1) Van der Waals, J.D. Over de Continuïteit van den Gas- en Vloeistofoestand (on the continuity of the gas and liquid state). *PhD thesis* **1873**.
- (2) Duong, D. L.; Yun, S. J.; Lee, Y. H. van der Waals Layered Materials: Opportunities and Challenges. *ACS Nano* **2017**, *11*, 11803-11830.
- (3) Kohn, W.; Sham, L. J. Self-Consistent Equations Including Exchange and Correlation Effects. *Phys. Rev.* **1965**, *140*, A1133-A1138.
- (4) Perdew, J. P.; Burke, K.; Ernzerhof, M. Generalized Gradient Approximation Made Simple. *Phys. Rev. Lett.* **1996**, *77*, 3865-3868; Erratum: *Phys. Rev. Lett.* **1997**, *78*, 1396.
- (5) Kohn, W.; Meir, Y.; Makarov, D. E. van der Waals Energies in Density Functional Theory. *Phys. Rev. Lett.* **1998**, *80*, 4153-4156.
- (6) Pernal, K.; Podeszwa, R.; Patkowski, K.; Szalewicz, K. Dispersionless Density Functional Theory. *Phys. Rev. Lett.* **2009**, *103*, 263201.
- (7) Stöhr, M.; Van Voorhis, T.; Tkatchenko, A. Theory and practice of modeling van der Waals interactions in electronic-structure calculations. *Chem. Soc. Rev.* **2009**, *48*, 4118-4154.
- (8) Ruiz, V.G.; Liu, W.; Zojer, E.; Scheffler, M.; Tkatchenko, A. Density-functional theory with screened van der Waals interactions for the modeling of hybrid inorganic-organic systems. *Phys. Rev. Lett.* **2012**, *108*, 146103.
- (9) Su, G.; Yang, S.; Li, S.; Butch, C. J.; Filimonov, S. N.; Ren, J.-C.; Liu, W. Modeling chemical reactions on surfaces: The roles of chemical bonding and van der Waals interactions. *Prog. Surf. Sci.* **2019**, *94*, 100561.

- (10) Foulkes, W.; Mitas, L.; Needs, R.; Rajagopal, G. Quantum Monte Carlo Simulations of Solids. *Rev. Mod. Phys.* **2001**, *73*, 33-83.
- (11) Raghavachari, K.; Trucks, G. W.; Pople, J. A.; Head-Gordon, M. A Fifth-Order Perturbation Comparison of Electron Correlation Theories. *Chem. Phys. Lett.* **1989**, *157*, 479-483.
- (12) Eshuis, H.; Bates, J. E.; Furche, F. Electron Correlation Methods Based on the Random Phase Approximation. *Theor. Chem. Acc.* **2012**, *131*, 1089-1102.
- (13) Medvedev, M. G.; Bushmarinov, I. S.; Sun, J.; Perdew, J. P.; Lyssenko, K. A. Density functional theory is straying from the path toward the exact functional. *Science* **2017**, *355*, 49-52.
- (14) Kasai, H.; Tolborg, K.; Sist M.; Zhang, J.; Hathwar, V. R.; Filsø, M. Ø.; Cenedese, S.; Sugimoto, K.; Overgaard J.; Nishibori E. et al. X-ray electron density investigation of chemical bonding in van der Waals materials. *Nature Materials* **2018**, *17*, 249-253.
- (15) Sabatini R.; Gorni, T.; de Gironcoli, S. Nonlocal van der Waals density functional made simple and efficient. *Phys. Rev. B* **2013**, *87*, 041108.
- (16) Blöchl, P. E. Projector augmented-wave method. *Phys. Rev. B* **1994**, *50*, 17953-17979.
- (17) Yourdshahyan, Y.; Zhang, H. K.; Rappe, A. M. n-alkyl thiol head-group interactions with the Au(111) surface. *Phys. Rev. B* **2001**, *63*, 081405.
- (18) Grimme, S. Accurate description of van der Waals complexes by density functional theory including empirical corrections. *J. Comput. Chem.* **2004**, *25*, 1463-1473.
- (19) Grimme, S. Semiempirical GGA-type density functional constructed with a long-range dispersion correction. *J. Comput. Chem.* **2006**, *27*, 1787-1799.
- (20) Becke, A. D.; Johnson, E. R. Exchange-hole dipole moment and the dispersion interaction: High-order dispersion coefficients. *J. Chem. Phys.* **2006**, *124*, 014104.

- (21) Dion, M.; Rydberg, H.; Schröder, E.; Langreth, D. C.; Lundqvist, B. I. Van der Waals Density Functional for General Geometries. *Phys. Rev. Lett.* **2004**, *92*, 246401.
- (22) Vydrov, O. A.; Van Voorhis, T. Nonlocal van der Waals density functional: The simpler the better. *J. Chem. Phys.* **2010**, *133*, 244103.
- (23) Murray, É. D.; Lee, K.; Langreth, D. C. Investigation of Exchange Energy Density Functional Accuracy for Interacting Molecules. *J. Chem. Theory Comput.* **2009**, *5*, 2754-2762.
- (24) Perdew, J. P.; Wang, Y. Accurate and simple analytic representation of the electron-gas correlation energy. *Phys. Rev. B* **1992**, *45*, 13244-13249.
- (25) Jurečka, P.; Šponer, J.; Černý, J.; Hobza, P. Benchmark database of accurate (MP2 and CCSD(T) complete basis set limit) interaction energies of small model complexes, DNA base pairs, and amino acid pairs. *Phys. Chem. Chem. Phys.* **2006**, *8*, 1985-1993.
- (26) Román-Pérez, G.; Soler, J. M. Efficient Implementation of a van der Waals Density Functional: Application to Double-Wall Carbon Nanotubes. *Phys. Rev. Lett.* **2009**, *103*, 096102.
- (27) Giannozzi, P.; Baroni, S.; Bonini, N.; Calandra, M.; Car, R.; Cavazzoni, C.; Ceresoli, D.; Chiarotti, G. L.; Cococcioni, M.; Dabo, I. QUANTUM ESPRESSO: a modular and open-source software project for quantum simulations of materials. *Journal of Physics: Condensed Matter* **2009**, *21*, 395502-395521.
- (28) Giannozzi, P.; Andreussi, O.; Brumme, T.; Bunau, O.; Buongiorno Nardelli, M.; Calandra, M.; Car, R.; Cavazzoni, C.; Ceresoli, D.; Cococcioni, M. et al. Advanced capabilities for materials modelling with Quantum ESPRESSO. *Journal of Physics: Condensed Matter* **2017**, *29*, 465901-465931 .
- (29) <http://www.quantum-espresso.org/pseudopotentials>

- (30) Charles, H. A.; Meyer, W. W. Optimal Error Bounds for Cubic Spline Interpolation. *Journal of Approximation Theory* **1976**, *16*, 105-122.
- (31) Otero-de-la-Roza A.; Blanco, M. A.; Pendás, A. M.; Luaña, V. Critic: a new program for the topological analysis of solid-state electron densities. *Comput. Phys. Commun.* **2009**, *180*, 157-166.
- (32) Otero-de-la-Roza, A.; Johnson, E. R.; Luaña, V. Critic2: a program for real-space analysis of quantum chemical interactions in solids. *Comput. Phys. Commun.* **2014**, *185*, 1007-1018 .
- (33) Peng, H.; Yang, Z. H.; Perdew, J. P.; Sun, J. Versatile van der Waals Density Functional Based on a Meta-Generalized Gradient Approximation. *Phys. Rev. X* **2016**, *6*, 041005.
- (34) Björkman, T.; Gulans, A.; Krasheninnikov, A. V.; Nieminen, R. M. van der Waals Bonding in Layered Compounds from Advanced Density-Functional First-Principles Calculations. *Phys. Rev Lett.* **2012**, *108*, 235502.
- (35) Clerc, D. G.; Poshusta, R. D.; Hess, A. C. Periodic Hartree-Fock Study of TiS₂. *J. Phys. Chem.* **1996**, *100*, 15735-15747.
- (36) Ambrosetti, A.; Reilly, A. M.; DiStasio Jr., R. A.; Tkatchenko, A. Long-range correlation energy calculated from coupled atomic response functions. *J. Chem. Phys.* **2014**, *140*, 18A508.
- (37) Ambrosetti, A.; Silvestrelli, P.L.; Tkatchenko, A. Physical adsorption at the nanoscale: Towards controllable scaling of the substrate-adsorbate van der Waals interaction. *Phys. Rev. B* **2017**, *95*, 235417.
- (38) Becke, A. D. Perspective: Fifty years of density-functional theory in chemical physics. *J. Chem. Phys.* **2014**, *140*, 18A301.

- (39) Troullier, N.; Martins, J. L. Efficient pseudopotentials for plane-wave calculations. *Phys. Rev. B* **1991**, *43*, 1993-2006.
- (40) Louie, S. G.; Froyen, S.; Cohen, M. L. Nonlinear ionic pseudopotentials in spin-density-functional calculations. *Phys. Rev. B* **1982**, *26*, 1738-1742.
- (41) Qin, Z.; Wang, L.; Cong, R.; Jiao, C.; Zheng, X.; Cui, Z.; Tang, Z. Spectroscopic identification of the low-lying states of S₂ molecule. *J. Chem. Phys.* **2019**, *150*, 044302.
- (42) Berland, K.; Hyldgaard, P. Exchange functional that tests the robustness of the plasmon description of the van der Waals density functional. *Phys. Rev. B* **2014**, *89*, 035412.
- (43) Grimme, S.; Antony, J.; Ehrlich, S.; Krieg, H. A consistent and accurate ab initio parametrization of density functional dispersion correction (DFT-D) for the 94 elements H-Pu. *J. Chem. Phys.* **2010**, *132*, 154104.

